SFWA

Final report

JTI-CS-SFWA-01-003
255752
Leading Edge Box Design for Swept Flow Control Wing

Prepared by: **Lead Contributors** **Peter Scholz (TU-BS)**
Claus-Philipp Hühne (TU-BS)
Saquib S. Mahmood (TU-BS)

1 Table of Contents

2 Introduction

This final deliverable presents key results that have been generated in the JTI/SFWA programme of the EC under Grant Agreement GA255752 in the CfP-project “Leading-Edge Box Design for Swept Flow-Control wing” (LEBox). This report is a technical report, which presents core results and highlights. For more detailed discussions the reader is referred to the individual and more comprehensive deliverables. In order to follow the logical scientific argumentation within LEBox the following order of deliverables is recommended:

No.	Title
D2.1	Concept Report
D2.2	Analysis of Previous Experiments
D1.1	Actuator geometry (Numerical results)
D3.1	Mid-Scale Tests Conducted and Analyzed (Discussion of experimental data)
D3.2	Comparison of Experimental and Numerical Results

It is noted here that D2.3 and D2.4 are so-called “O-type” deliverables, which means they do not exist as a full report, but rather in terms of existing hardware.

The main objective of LEBox was to demonstrate the potential of flow control at the leading edge of a swept airfoil, i.e. to suppress a turbulent flow separation at high angles of attack and thus increase maximum lift of the configuration. The configuration that was chosen during project preparation is the DLR F15 airfoil. Therefore, within the CfP-project, an intensive and fruitful collaboration with the owner

of the respective model, DLR/AS Braunschweig, has been established. Based thereon, the DLR-F15 model was available in the beginning as a (till then: non-swept) modular windtunnel model. The DLR-F15 was supposed to be used in a “slatless” two-element configuration consisting of an airfoil main element and a gapped trailing edge fowler flap. Regarding the choice of the high-lift flap configuration the relevant partners (which are: TU-BS within this CfP-project, TU Berlin, who will do active flow control at the flap within their CfP-project “AFC-TEFL-HLC” in the same windtunnel entry and DLR who is the main point of contact for these tests and serves as an interface between the windtunnel DNW-NWB and the two CfP partners) pre-selected one configuration, which was known from background knowledge, see [2-6], to serve as a good reference for L/E as well as for T/E flow control studies. In internal communication called “flap setting #2, fs#2”, the configuration is defined as follows:

Flap gap g_F	2.7 % (*)
Flap overlap ovl_F	0.5 % (*)
Flap angle	45°

(*) of reference chord, c_{ref} = 600 mm

In terms of the flow control technique the use of a row of vortex generating jets (VGJs) at the leading edge was proposed, as used in several preceding studies [1,2,4,5]. Such VGJs basically consist of small orifices slightly upstream of the airfoil leading edge, though downstream of the stagnation point. The orifices are circular holes, pitched and skewed with respect to the oncoming flow, to create a local streamwise vortex structure. The vortex structure enhances the turbulent mixing inside the boundary layer and is therefore able to suppress a turbulent separation.

LEBox was split in three work packages. WP1 deals with numerical evaluation of flow separation control at the airfoil leading edge by means of a state-of-the-art RANS solver. WP2 was about the concept design, manufaction of components and preparation of the mid-scale windtunnel tests in DNW-NWB. Finally in WP3 the windtunnel test was accomplished and the data has been analyzed and put into contest.

In this document, the chapters follow the work package structure, which does not necessarily equal the timeline of the individual tasks, however, hints on workpackage-interaction are given where it seemed convenient. Basically, this report is a compilation of the technical part of the two periodic reports submitted to the SFWA management. Also it might be noted, that this report is identical to the last LEBox-deliverable D0.1, also named “final report”.

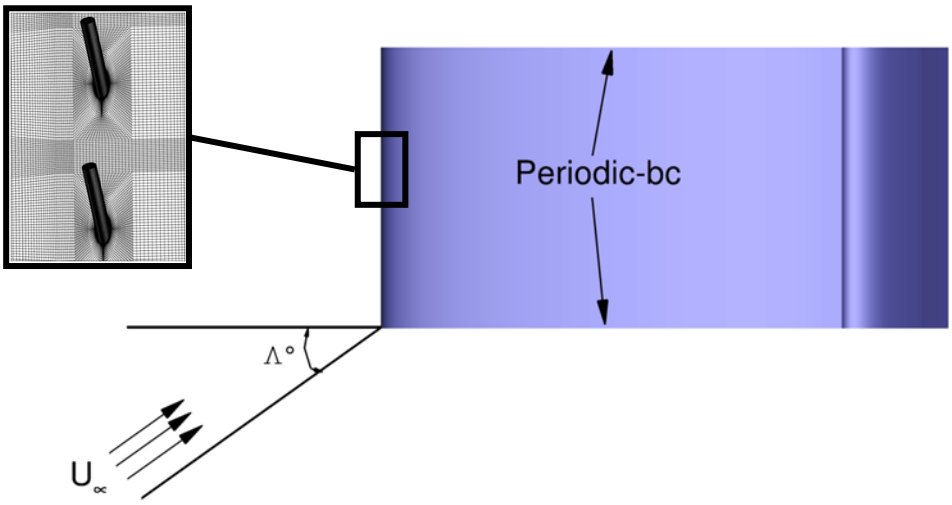

Figure 1: Setup for the 2.5D computations, using a full 3D grid with periodic boundary conditions and oblique inflow

3 Numerical Evaluation of L/E-Flow Control

3.1. Objectives of WP1

The objectives of the numerical studies within LEBox were to find effective and efficient geometrical configurations for the VGJ orifices, in terms of pitch- and skew angles and orientation. Since the leading edge boundary layer was expected to be significantly twisted as an effect of the airfoil sweep, the geometrical parameters have been fairly unknown—although experiences existed from non-swept airfoil studies, e.g. [1-5]. It was expected that the twisted boundary layer will "favor" one sense of rotation of the local vortices and thus amplify them and it was intended to utilize this effect. Beside evaluation of different geometrical variants, the numerical studies have been utilized to extrapolate the effect of the VGJs to higher Reynolds numbers.

3.2. Numerical Setup

RANS computations have been performed on a fully 3D multi-block structured mesh consisting of approximately $13 \cdot 10^6$ grid points. The mesh resolves the airfoil, including the high lift flap and the VGJ orifice located at the leading edge. Grid generation has been carried out using the commercial software GRIDGEN V15.1. Fig. 1 shows the arrangement for the DLR F15 high-lift airfoil with a sweep angle of Λ=30°. The flow control computations have been performed with spanwisely periodic boundary conditions, thus the case effectively represents a slice of an infinite aspect ratio swept airfoil (2.5D-computations), although the local 3D-structures emanating from the VGJ-orifices are fully resolved and therefore require a full 3D grid. It must be noted that the flow solutions for reference cases (no flow control) have been generated on a 2D grid, using a 2.5D-approach with oblique inflow.

For the modeling of the VGJs a certain "length" of the orifice has been meshed (see Fig. 1), at the end of which a special actuation boundary condition was applied. By doing so, the VGJs can be operated with a specific mass flow rate and thus jet exit flow velocity, or C_μ, respectively. It must be noted that, though in the experiments the actuators can be run with static blowing, as well as with dynamic blowing, the simulation of dynamic blowing is not possible with reasonable effort. Therefore the numerical simulations only cover static blowing. It must be assumed here that the variation of effectiveness of different VGJ geometries holds for dynamic blowing.

All computations were conducted at a free stream Mach number of Ma=0.15 with the Reynolds number of $Re=2.0 \cdot 10^6$ based on the reference chord length. Grid convergence was ensured with comparative simulations, also the validity of the turbulence model (Spallart Allmaras SAS one equation model) was validated against experimental data.

Reference computations have shown airfoil stall at AoA=9°. To assess the effect of different VGJ configurations comparative simulations were performed. To achieve convergence each of the simulations made use of a time stepping scheme, e.g. the results represent a quasi-steady time average, but the computations themselves are fully time resolved. Due to this significant computational

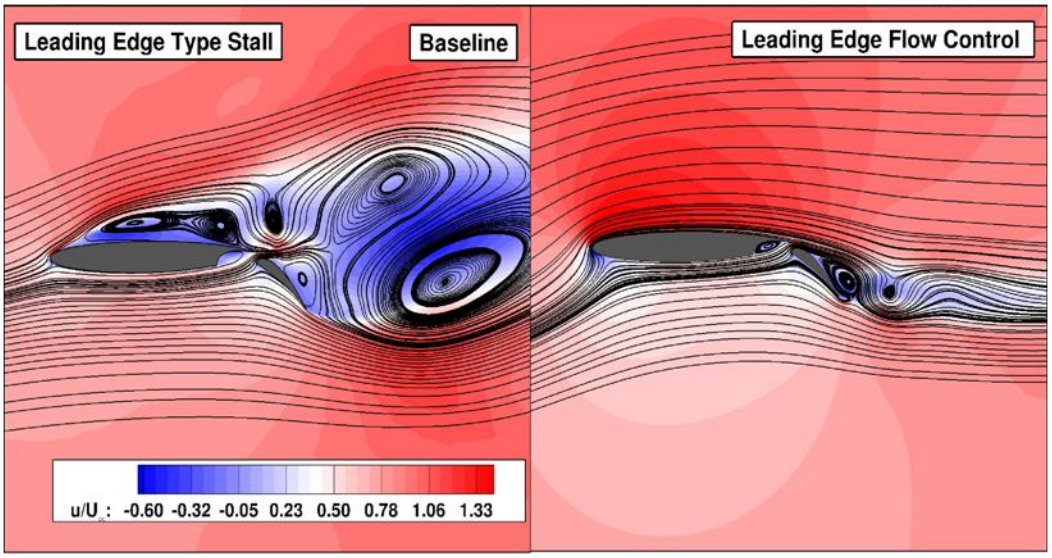

Figure 2: Flowfield streamline visualization at AoA=9.5° for the baseline case and an actuated case

effort it is not efficient to generate full lift curves for each VGJ configuration, but rather simulations were done at one single AoA=9.5°. The effectiveness of the different configurations is then assessed by comparing the resulting pressure distribution, wall shear stress and vortex properties (e.g. vortex strength and position).

3.3. Results

At first, to highlight the general ability of the numerical approach to assess leading edge flow control, Fig. 2 shows streamline plots of two computational results: The left figure shows the results for a baseline case. It is clearly visible that the flow separates right at the leading edge of the airfoil. The right part of the figure shows the same conditions, but with L/E-AFC activated (configuration: “favr.VGJ-1d”, explanation will be given below). It is clearly visible that the numerical approach is able to predict a turbulent leading edge stall (which in itself is a challenge), as well as the general effect of the L/E-AFC-system.

In order to find an advantageous geometrical VGJ configuration, comparative computations with different variants of VGJs have been performed. The variations covered the following range of geometries: co-rotating VGJs, oriented with favorable (favr) and unfavorable (unfavr) sense of rotation, counter-rotating arrays (ctr-rot), different spanwise spacings (5d, 10d, 20d), different skew (β=90°, 75°, 105°), different pitch (α=30°, 15°), different velocity ratios (VR=5, 4.5, 5.7) and different combinations thereof.

For a quick glance Fig. 3 (a) shows the lift curve computed for the reference case, as well as four selected configurations of the VGJs, which—as mentioned before—have been performed at one AoA only and therefore appear as single points in the diagram. Furthermore Fig. 3 (b) shows the results of all variants as a comparison of the lift coefficient at AoA=9.5°. All different variants were actually able to suppress the leading edge stall that was observed for the baseline case. However, since the vortices that are generated by the different VGJs variants differ in size and position, they do feature differences in the C_L that is actually achieved by the respective configuration as can be seen in Fig. 3 (b). Again, it is worthwhile to note that the approach that was chosen in LEBox proved to be efficient, delivered feasible results and showed that it is sensitive enough to assess even rather small differences between configurations: This is highlighted here by a comparison of the local pressure distribution C_P and the distribution of the wall shear stress coefficient C_f in Fig. 4. The configurations shown in Fig. 4 are, beside the baseline case: “favr VGJ-10d”, which typically served as a “standard reference” during the comparisons, because it equals the configuration that has been used in previous 2D-studies. “favr VGJ-10d-α=15°” is a configuration, where the pitch angel of the VGJs has been reduced from 30° to 15° to place the vortices closer to the airfoil surface. “favr VGJ-10d-β=105°” is a configuration where the skew angle has been increased from 90° to 105°, which ensures that the VGJs are perpendicular to the local flow streamlines, which , since the airfoil is swept, does not

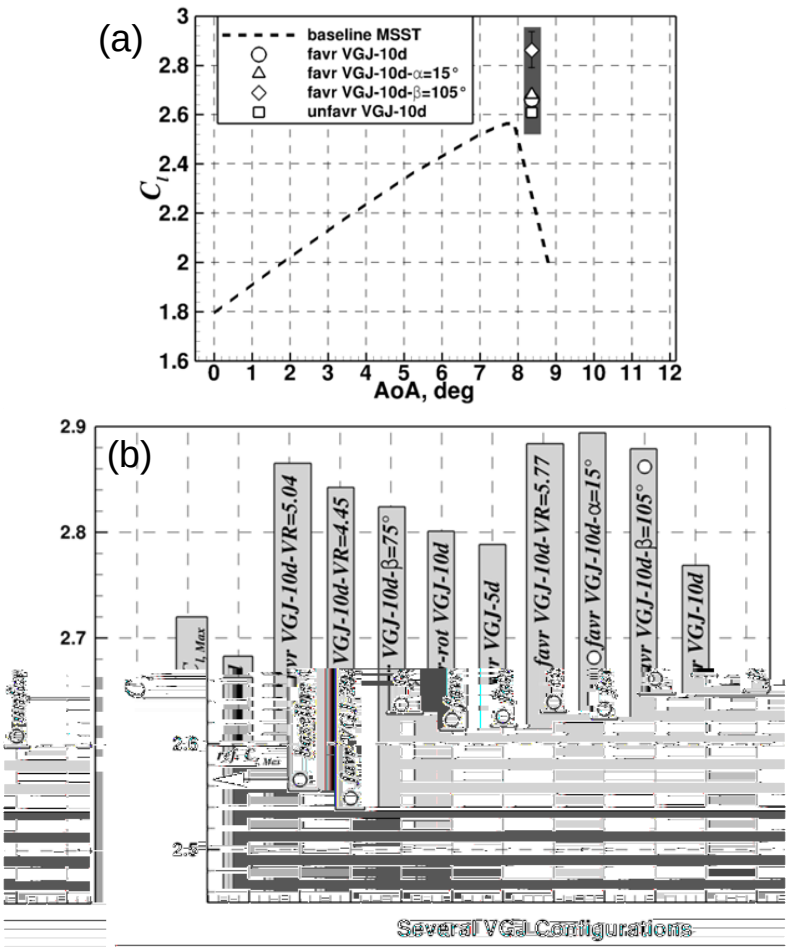

Figure 3: (a) Lift curve with reference (baseline) case and four different AFC cases; (b) detailed comparison of various AFC cases

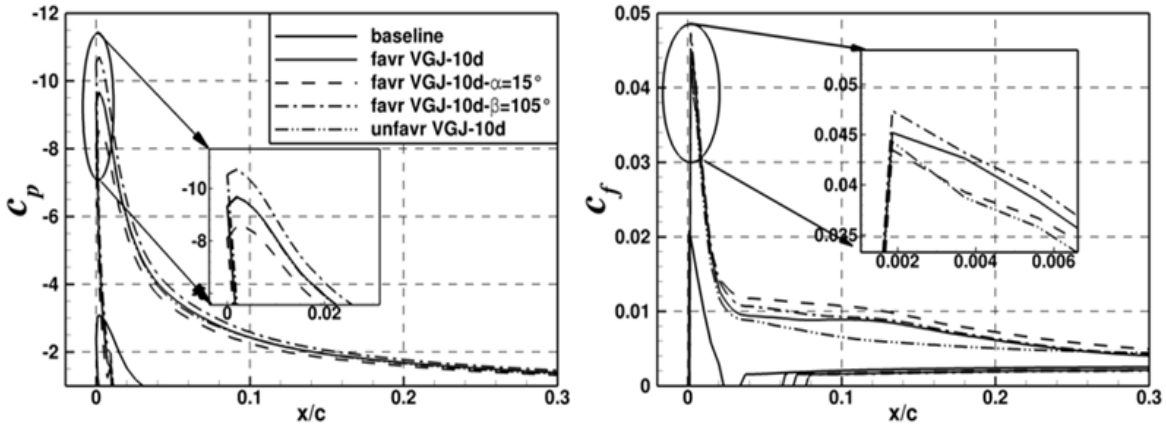

Figure 4: Detailed comparison of selected cases in terms of (left) pressure distribution $C_P(x/c)$ and distribution of wall shear stress coefficient $C_f(x/c)$ in the leading edge region of the airfoil

mean that the VGJs are perpendicular to the airfoil's leading edge. Finally, "unfavr VGJ-10d" serves for comparison, because it is expected to give unfavorable results.

As can be seen from Fig. 4, the numerical scheme is well able to distinguish between such configurational changes, since e.g. the unfavorably rotating case "unfavr" is indeed not advantageous ("advantageous" means here, that C_p is small—e.g. larger lift force—and C_f is large—e.g. the flow is "far" from separation). On interesting detail can be found in this comparison: While it seems that the case "favr VGJ-10d-β=105°" is more advantageous in the very leading edge region x/c<0.005, for a region further downstream the configuration "favr VGJ-10d-α=15°" becomes better. It was yet unkown, which of the two effects might finally be more advantageous in terms of overall maximum lift, since this comparison is at one given AoA. Therefore for these two VGJ configurations some additional AoA were computed to show up the effect on maximum lift and AoA.

The respective results are shown in Fig. 5. It seems that the two configurations have a quite different phenomenology of stall prevention, since their near-stall behavior is quite different. While "favr VGJ-10d-α=15°,β=90°" acts more as a linear extension of the lift curve, the other configuration "favr VGJ-10d-α=30°,β=105" introduces one significant increase of lift at a certain AoA of approximately 8.5°, but then lift reduces with increasing AoA,

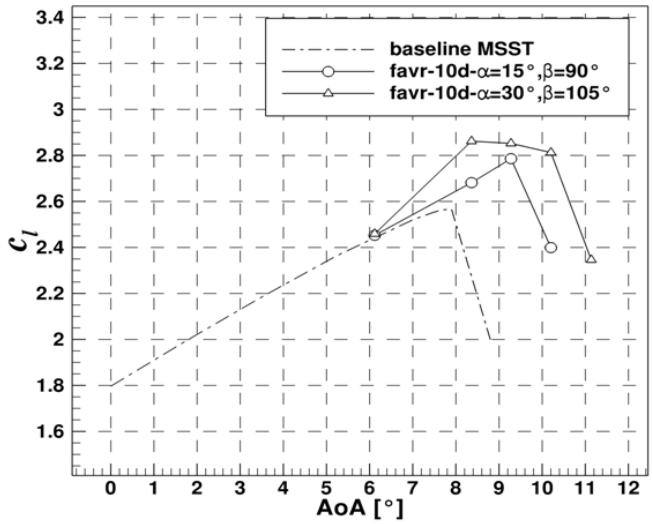

Figure 5: Computed lift curves for the two most promising VGJ configurations

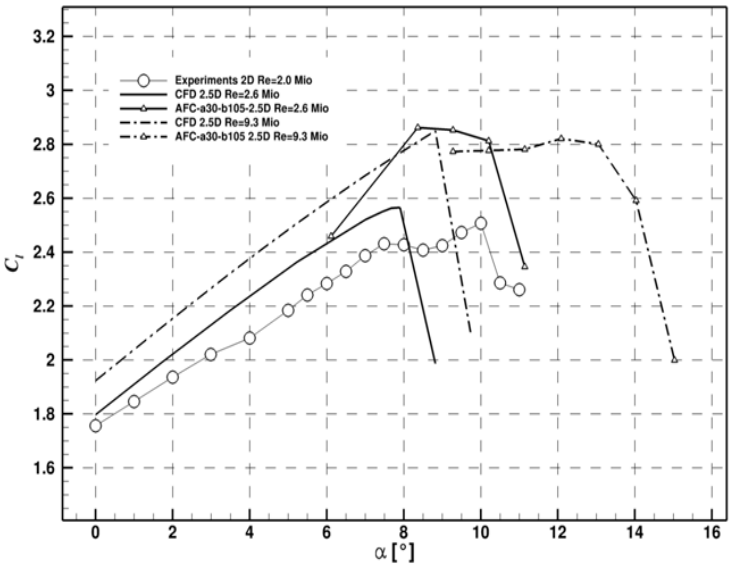

Figure 6: Computed lift curves and extrapolation of AFC results to higher Re

though being always larger than the lift of the other configuration with α=15°,β=90°. Despite its somehow stranger behavior, based on these results the configuration was chosen, which delivers larger overall maximum lift, which is: VGJs rotating in “favorable” direction (against the local twist of the boundary layer), pitch angle α=30°, skew angle β=105°. The latter is measured relative to the swept leading edge tangent, the slightly increased skew of 105° instead of 90° ensures that the VGJs operate perpendicular to the local flow direction, since the flow locally skews a bit less than the airfoil.

As a last step the results have been extrapolated to higher Reynolds number. Re=9.3 Mio was used, which is the design Re number of the DLR-F15 airfoil. The result in terms of lift over AoA is shown in Fig. 6. It turns out that at higher Re number the effectiveness (in terms of maximum lift coefficient) of the AFC stays the same, whereas the maximum lift of the reference case increases with increasing Re as expected, thus the relative effect of the AFC in terms of lift decreases. The effect of the AFC system in terms of maximum angle of attack however increases with increasing Re, such that at low Re one can find AoA_{max}≈10°, but at higher Re AoA_{max}≈14°. Thorough investigation of the flowfields yields that the AFC system also at higher Re is still able to maintain the leading edge suction peak. Thus the L/E-AFC is successful. It can be shown that at higher Re and AoA between 10° and 14° the airfoil shows a local separation at the trailing edge, which progresses upstream with increasing angle of attack. Therefore the limited effect at higher Reynolds numbers is not due to a reduced effectiveness of the AFC itself, but because of a different stalling mechanism.

4 Model Setup and L/E-Box-Design

4.1. Objectives of WP2

Originally, the objectives of the second work package are mainly to design and manufacture the L/E-Box for the windtunnel model with the AFC system included. However, very early in the project it turned out that the overall concept of a swept integration of the windtunnel model into the windtunnel was rather unclear—although this task in principle is part of the workshare of the partner DLR, many questions were completely unclear and almost no design work could be started before the concept was clear. Therefore significant workshare was put into the conceptual design of the experimental setup. While DLR focused on the design and connection of the model to the existing infrastructure of the windtunnel (e.g. rotating tables), TU-BS designed and performed studies on the shaping of the wingtip device and on the aerodynamic influence of the windtunnel in the swept arrangement.

4.2. Concept for Model Integration

During project proposal and negotiation some different wind tunnel integration methods have been presented that are shown in Fig. 7. In order to focus on one of these different variants, each of them has been evaluated against certain criterias:

	Wall-to-wall	Swept constant-chord	Struts
Expected quality of results	+/-	+	-
Structural integrity	+	+/-	-
Supply of pressurized air	-	+	-
Model assembly	-	+/-	+
Realizable sweep-angle range	-	+	+

It should be noted that of course the overall objective of the project is to enable high-quality measurements of a 2.5D-airfoil-case. Some key arguments will be discussed in the following.

The expected quality of the results is not good with the strut integration, since they will significantly disturb the flow. The wall-to-wall-integration was expected to suffer from significant problems with local separations in the “upper” corner, where the wing appears to be “swept forward” with respect to the windtunnel sidewall. Such forward swept arrangements will lead to an increase of local suction peaks at the airfoil in the intersection region. Thus the setup might pronounce stall effects that are not realistic for a 2.5D-airfoil. Although the wall-to-wall-integration is somewhat geometrically “more similar” to a 2.5D-case it was therefore expected, that better results can be achieved with a swept

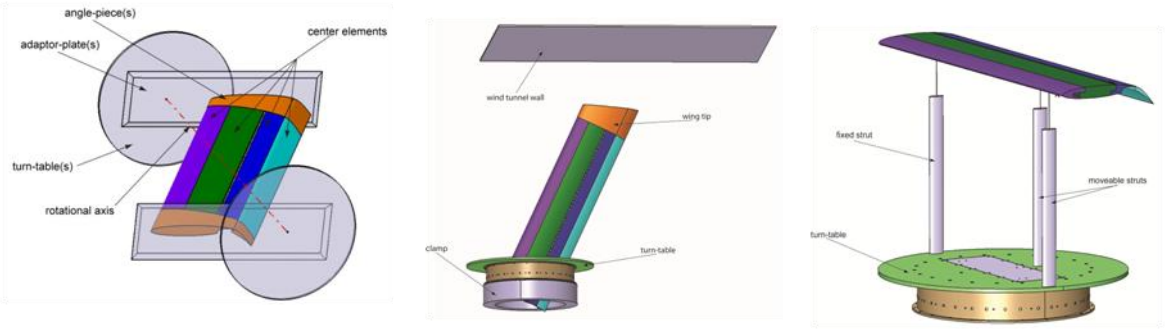

Figure 7: Sketches of the different integration possibilities studied together with DLR;
From left to right: (1) wall-to-wall-integration, (2) swept constant-chord setup, (3) strut-setup

constant chord setup: Since there is no forward swept wall interface, local separations are limited to the wingtip region. Hence, at some distance from the wall and from the wingtip better quasi-2.5D-conditions can be found than with the wall-to-wall-integration.

Though this was the most important argument, the following issues have also been found to be advantageous:

A goal was to reach a sweep angel in the range of 20° to 30°, where a greater angle is preferred because of the stronger three dimensional behavior of the boundary layer. The swept constant-chord integration allows sweep up to 30°, while the wall-to-wall-integration concept would be limited to less than 20°. Also (at least in principle) a variation of the sweep angle is possible by rotating the wing around the pendulum bearing.

The model assembly and supply of pressurized air of the swept constant-chord integration is less complex and expensive, compared to the wall-to-wall integration. That is attributed to the complex adapters, which must be provided for a wall-to-wall integration to connect to outer models to the turning plates of the windtunnel.

4.3. Wingtip-Design

For the swept constant-chord integration however a suitable wingtip is needed to cover the free wing end. This is necessary to reduce separation effects at the outer wing. This wingtip device had to fulfill different requirements. First, there should be enough space inside the wingtip for a pressure supply connection between the main element and the flap. Second, the wingtip should influence the flow around the wing positively and should show no or at least only weak local separations at the wingtip.

To design a wingtip tank and also to gather comparative data including all the effects of sweep, finite span and windtunnel environment, which can be used to transfer and/or extrapolate results in between

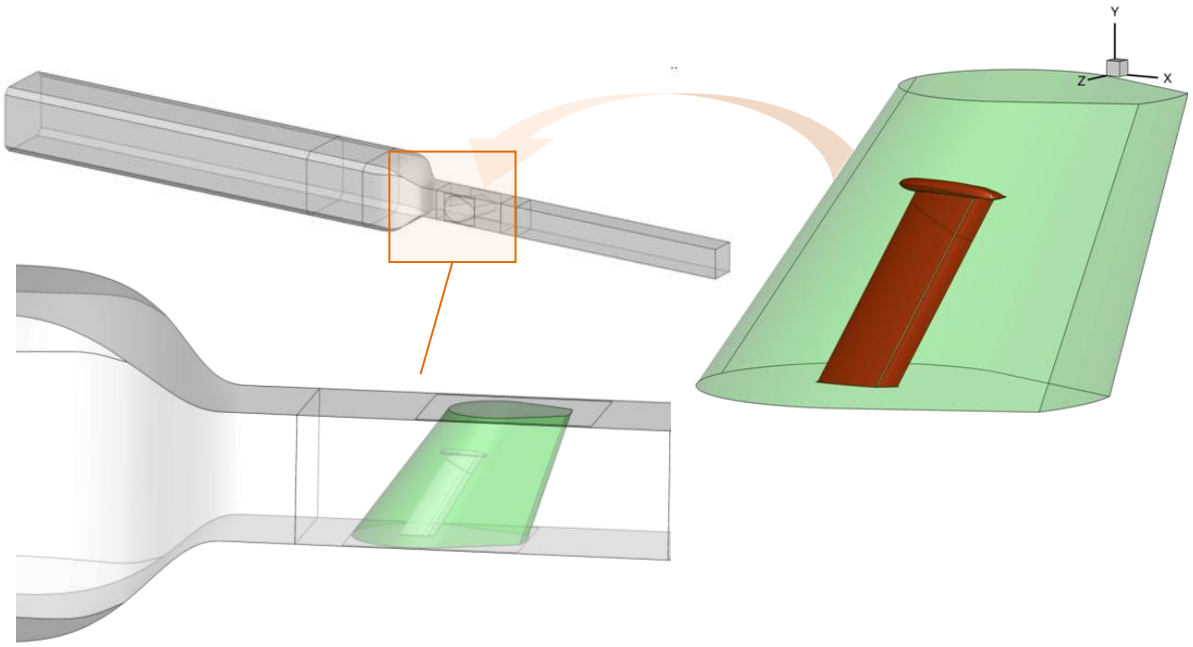

Figure 8: Numerical representation of the wind tunnel (upper left), the airfoil with the inner grid (upper right) and the airfoil inside the windtunnel (lower)

the 2.5D-computations and the experimental (3D) results, 3D-numerical computations have been performed (full wing with sweep, w/o flow control), which represent the full wing inside the windtunnel test section, as well as under “farfield conditions”.

The wing was placed into a windtunnel representing the same setup as used during the experiments. To allow for an efficient modification of the angle of attack of the model inside the windtunnel a chimera approach with two different grids was used: The “outer” windtunnel grid consisted of approximately 1 Mio cells, discretizing a rather long inflow section, the windtunnel nozzle, the windtunnel test section and an outflow section. The “inner” wing grid discretized the swept constant

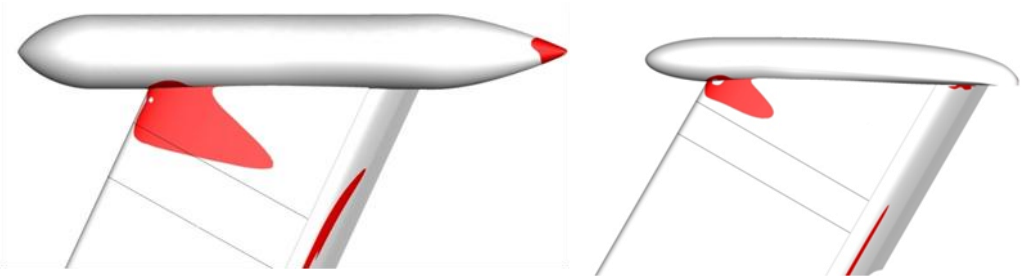

Figure 9: Comparison of two different tip tank versions. Red areas denote reversed flow direction (separation)

chord setup of the airfoil/wing model, framing the wing up to approximately one chord length upstream, two chord lengths downstream and two chord lengths in spanwise direction. The inner grid can be placed into the outer grid, where the grids are then coupled by an interpolation framework (Chimera-technique). This allows changing the AoA of the wing while using the same grids. Also this setup allows to change the airfoil model (e.g. for variation of wingtip-style). In total the setup consists of approximately 11 Mio nodes (1 Mio windtunnel, 10 Mio inner grid). Additionally studies have been done with the 3D wing without windtunnel in “farfield conditions”, where the windtunnel grid is not existent and the inner grid extents into the far field.

Fig. 9 shows exemplary results of two tip tank versions. The left one is a geometrically simple, almost cylindrical part, the right one is a specifically designed version. The red areas denote regions with negative u-velocity component, e.g. separated areas. It can be seen that the specific design of the tip tank significantly reduces the separated areas. However, a completely attached flow was not achieved, basically because the tip tank required a certain volume to house pressure tubings in the inside.

4.4. Actuation System and L/E-Box Design and Modifications

A sketch of the actuator system is shown in Fig. 10, it basically consists of the valves fed by a pressure supply line, the settling chambers and the actuator orifice, which is manufactured into an “insert” that physically closes the settling chamber. One of the tasks was to find a technically feasible solution to achieve “filled” actuator chambers in the existing L/E-box. It has been found that filled actuator chambers are superior over the existing ones, which had “setting chambers” of a certain volume. After comprehensive testing the settling chambers of the existing L/E-Box were modified by the following steps:

1. Carefully remove existing actuator inserts, that cover the settling chambers (without implicating the L/E-box itself).

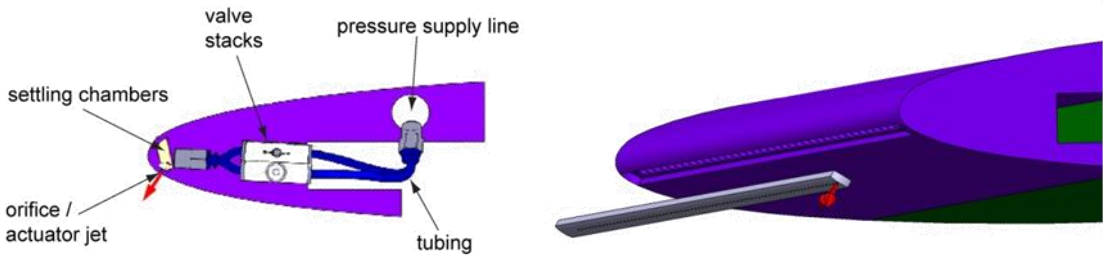

Figure 10: Sketch of the actuation system (left) and integration of insets into L/E-Box (right)

2. Fill the chambers with a very defined amount of thixotroped epoxy resin.
3. Close the filled chambers with “new” insets.

Also, manufaction and integration of the new actuator inserts with the VGJ-geometry found in WP1 was done. The inserts are milled from small aluminum sheets. The oblique actuator holes (with defined pitch and skew angle) are drilled using a 5-axis CNC-mill, in order to guarantee a very high quality of the holes (geometry see chapter 3 in this document).

The complete system to generate dynamically pulsing air jets with the VGJs has been modified and renewed. New fast switching valves (FESTO MHJ9 instead of FESTO MHE2) allow frequencies up to 1 kHz, instead of 300 Hz. This also required a replacement of the complete electronics behind the valves, including the frequency generator and the power electronics.

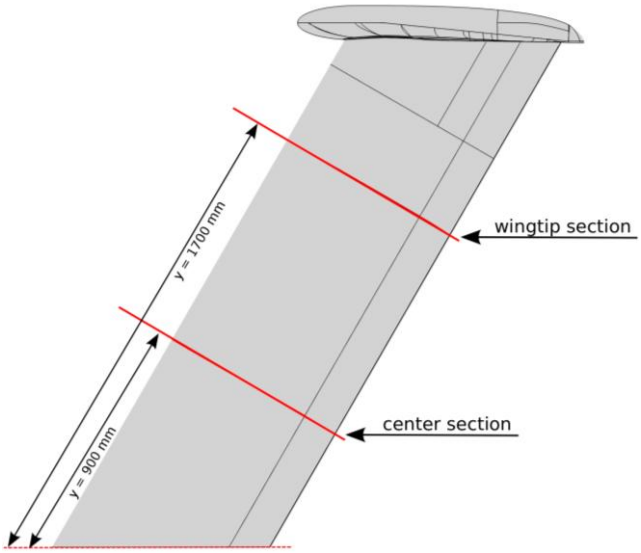

Figure 11: Sketch of the position of the two tap-sections, the outer one is retrofitted into the L/E-Box

Since the model setup concept is to use a finite constant-chord setup, it was found advantageous to have a means to monitor the spanwise change of pressure distribution. The windtunnel model itself is modular and one sectional row of pressure taps already existed in the center piece of the model, close to the wingtip (refer to Fig. 11). To fully exploit these existing taps, new taps had to be integrated into the L/E-Box to close this pressure section. This has been done by eroding new taps into the L/E-Box. It must be noted that this required very intensive planning and preparation, because the L/E-box is equipped with the actuation system shown in Fig. 10 thus there is barely any space for the tapping or the instrumentation with tubes.

As preparation for efficient windtunnel testing also a fully computer controlled setup of the pressure supply system was designed and build. Here, several supply pressures as well as valve frequencies and duty cycles can be controlled from the windtunnel control room, mass flow is measured and monitored and also a control loop allows holding certain values constant (e.g. mass flow, pressure or preliminary c_μ). The system was set up and tested extensively. It should be noted that the test itself was accomplished very efficiently, the system proofed to be robust and not a single failure or misoperation has been recognized over the two weeks of the entry.

5 Experimental Demonstration of L/E Flow Control

5.1. Objectives of WP3

The last work package in LEBox is dedicated to the experimental testing and data analysis. In the original planning several tasks were foreseen that were finally rearranged, as discussed in the periodic reports and individual deliverables. The core objectives of WP3 have however not been changed, that are to participate at the windtunnel entry, operate the L/E-AFC-system and analyze the data with respect to the demonstration of L/E-AFC-capability.

5.2. Experimental Setup

The experiments were performed in the Low-Speed Wind DNW-NWB Braunschweig, Germany, a Göttingen type of wind tunnel with a closed 3.25m x 2.8m test section. The measurements made use of the DLR-F15 model. This is a modular constructed wind tunnel model consisting of four parts: leading edge box, main centre-element, shroud and flap. The three parts of the main wing are made of high strength aluminium (Weldural – AlCu6.5Mn0.3) and the flap is of glass-fibre reinforced plastic (GFRP). Flap tracks allow a variable positioning of the flap. As mentioned in sections 2 and 4, within LEBox this nominal 2D-model was integrated as a swept constant-chord setup. Sweep angle was 30°.

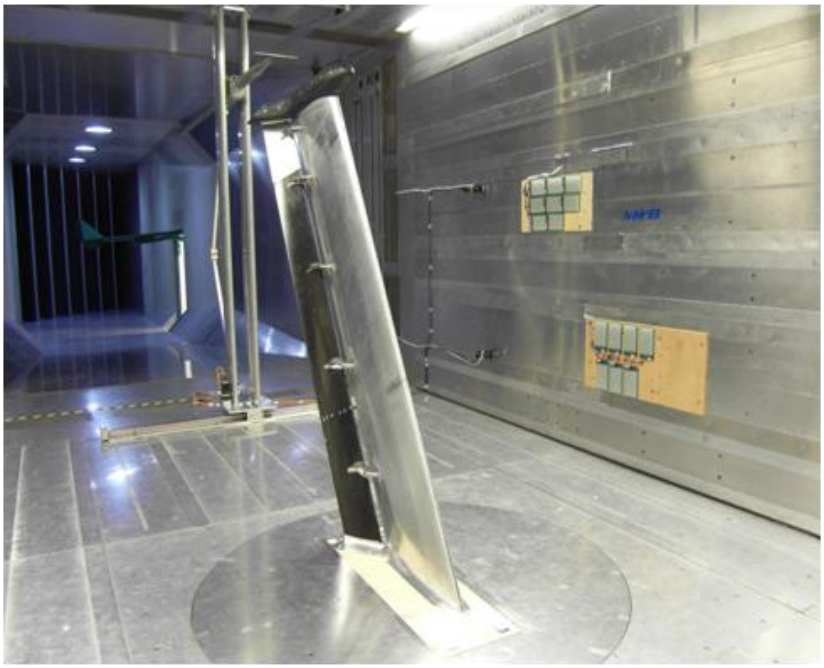

Figure 12: Swept constant-chord DLR-F15 model (Λ = 30°) in DNW-NWB test section

Due to the rather small Reynolds number a small-scale laminar separation bubble might be present at the L/E, which can result in a corresponding bubble-burst kind of stall. To prevent any laminar separation the transition was tripped by a thin 50 µm tape (2mm x 0.8mm). The rear edge of the tape strip was located at x/c=0%.

The pressure distribution was measured in two chordwise sections of pressure taps at the main wing and one at the flap. The centre tap section consists of 85 pressure taps (main wing + flap). This section was used to integrate the lift coefficient C_L that will be presented. Additionally a second tapping row is integrated near the tip with 40 pressure taps, to capture the three dimensional effects along the span. The outer tap section is however only available at the main element due to practical restrictions.

The windtunnel entry was effectively carried out from 10th Nov. 2011 to 30th Nov. 2011. Alfa-sweeps of a total of 322 cases have been measured, 19 of which have been reference cases (without active flow control), 129 have been dedicated to testing of the L/E flow control system. The remaining 174 were for the CfP-project “AFC-TEFL-HLC”, which used the same entry for their tests. The majority of the test cases has been done with a tunnel velocity of 60 m/s, which gives Re=2.0 Mio, Ma=0.15 (based on airfoil chord normal to L/E).

Pressure distributions and lift coefficients are given in a reference system normal to the L/E. Mini-tufts have been attached to the airfoil suction side and monitored with two digital cameras to gain insight into the stall behavior, mainly focusing on the wingtip area.

5.3. Core Results

Fig. 13 shows a comparison of the lift curves for the DLR-F15 model in unswept configuration (2D, taken from background data, refer to e.g. deliverable D2.2) with the recent data taken in the experimental entry of LEBox in the constant-chord setup. The 2D-lift is transferred into the swept using trigonometric functions. Fig. 13 clearly shows that the chosen setup delivers reproducible results. As a matter of fact, the intention of the setup is to enable high-quality testing of a quasi-2.5-airfoil, especially at AoA closed to stall. This objective was fully achieved, since the lift curves coincide very well. It should be noted that also the pressure distribution at higher AoA shows good comparison (refer to deliverable D3.1). The “kink” in the 2D-curve between AoA of 7°/8° comes from a reorganization of local separations (e.g. sidewall separations) that appear in the 2D setup. The 3D airfoil is slightly more robust

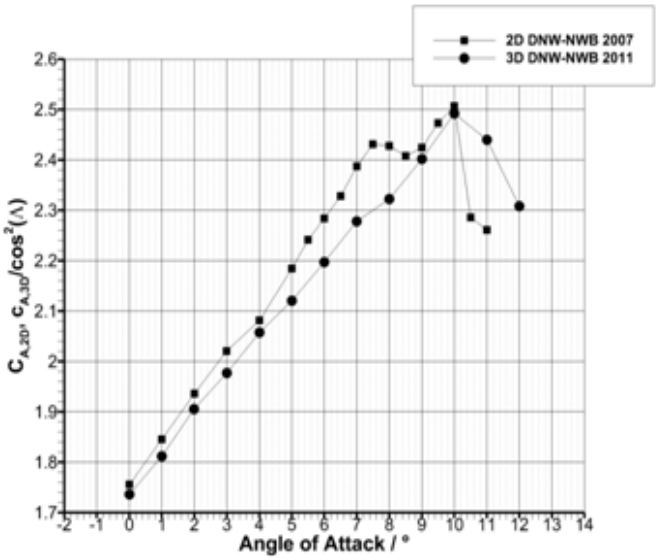

Figure 13: Comparison of (unswept) 2D results and 3D constant-chord results

to such separations, because of the sweep. It should however be noted that on the other hand the 3D setup shows some local separations at the wingtip. Also, for the case shown in Fig. 13 it has been observed by the tufts attached to the airfoil suction side, that the separation starts at the intersection of the wingtip-tank with the airfoil and then progresses “towards the root” with increasing AoA.

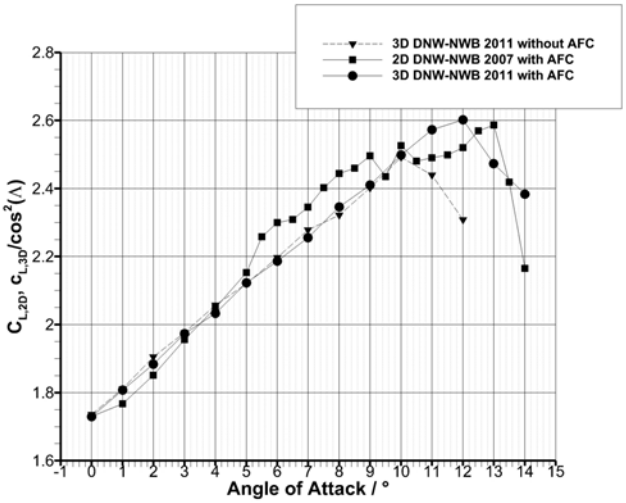

Figure 14: Lift over AoA for the 2D and 3D DLR-F15 airfoil without and with AFC (c_μ=0.48, F^+=0.87, dc = 50%)

Fig. 14 shows the 3D-reference case (without AFC) already discussed in Fig. 13, along with the curves with active flow control at the airfoil leading edge. One of the curves represents typical results from 2D testing (background knowledge) measured during a DNW-NWB entry in 2007, while the remaining curve is a recent result of the 3D testing (same C_μ, F^+ and dc as in 2007 with the 2D setup). Despite the swept setup the L/E-AFC-system is still able to recover the same lift as in 2D experiments. As mentioned above, again, the 3D lift curves are more “even” or “stable”, because the typical “swapping” of local separations that occurs in 2D testing is not so severe in the 3D setup.

Note, again, that these are some exemplary results, since the full analysis of the data is offered in deliverable D3.1 and is beyond the scope of this final report.

The basic conclusions from comprehensive variation of the flow control parameters are as follows:

- AFC generates a significant benefit in a regime where the flow can be assumed as 2.5D with a twisted boundary layer. The benefit is rather limited, when the separations are induced by other phenomena (e.g. near the wingtip)
- The stall mechanism is sensitive to the AFC parameter setting. The AFC might work as a separation control device (as it has been designed), but it might as well work as a post-stall flow control, if the separation cannot be prevented
- Frequencies higher than F^+=4 have no further advantage in terms of maximum lift.
- The α_{max} depends on the momentum coefficient and rises with increasing c_μ. However, at some specific c_μ a “transition point” is reached and α_{max} starts to decease with increased c_μ.
- For a given/requested efficiency, an increase of the momentum coefficient must be associated with a reduction of the reduced frequency F^+.
- With the “right” (dynamic) AFC parameter setting, nearly the same benefit can be produced as with other settings with substantially less energy.

Also, detailed comparisons of the experimental and the numerical results have been done and compiled into deliverable D3.2. Fig. 15 shows such exemplary comparison (Note that here the results are “unmodified”, e.g. not transformed into a reference system normal to the leading edge, because here all results represent an exact or quasi 2.5D case). The numerical results are described above and in detail discussed in deliverable D1.1, the experimental setup has also been described above and in detail in deliverable D3.1. As a conclusion, the reference cases without AFC show a rather good comparability between the experiments and the numerical simulations (pressure distribution will be compared later). However, the performance of the flow control system is significantly overpredicted in the numerical simulations, also the appearance of the resulting lift curves with active flow control seems to differ between experiment and numerics.

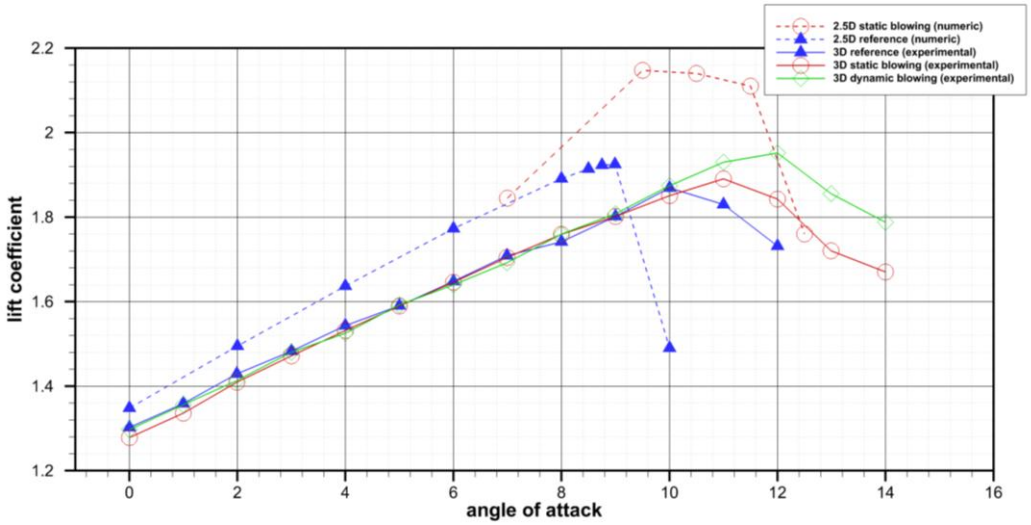

Figure 15: Lift coefficient vs. angle of attack, cases with flow control; comparison of experimental and numerical results (all AFC cases: $c_\mu \approx 1.45$)

Finally, to reveal an insight into the details the pressure distributions of these cases are shown in Fig. 8. Here a comparison of the C_P-distributions of the respective maximum-lift-cases is offered, hence by comparing the AFC cases to their respective reference, the effect of the AFC-system and the phenomenology of the stall control mechanism becomes visible.

At first attention should be drawn on the phenomenology of the dynamic blowing case. In contrast to

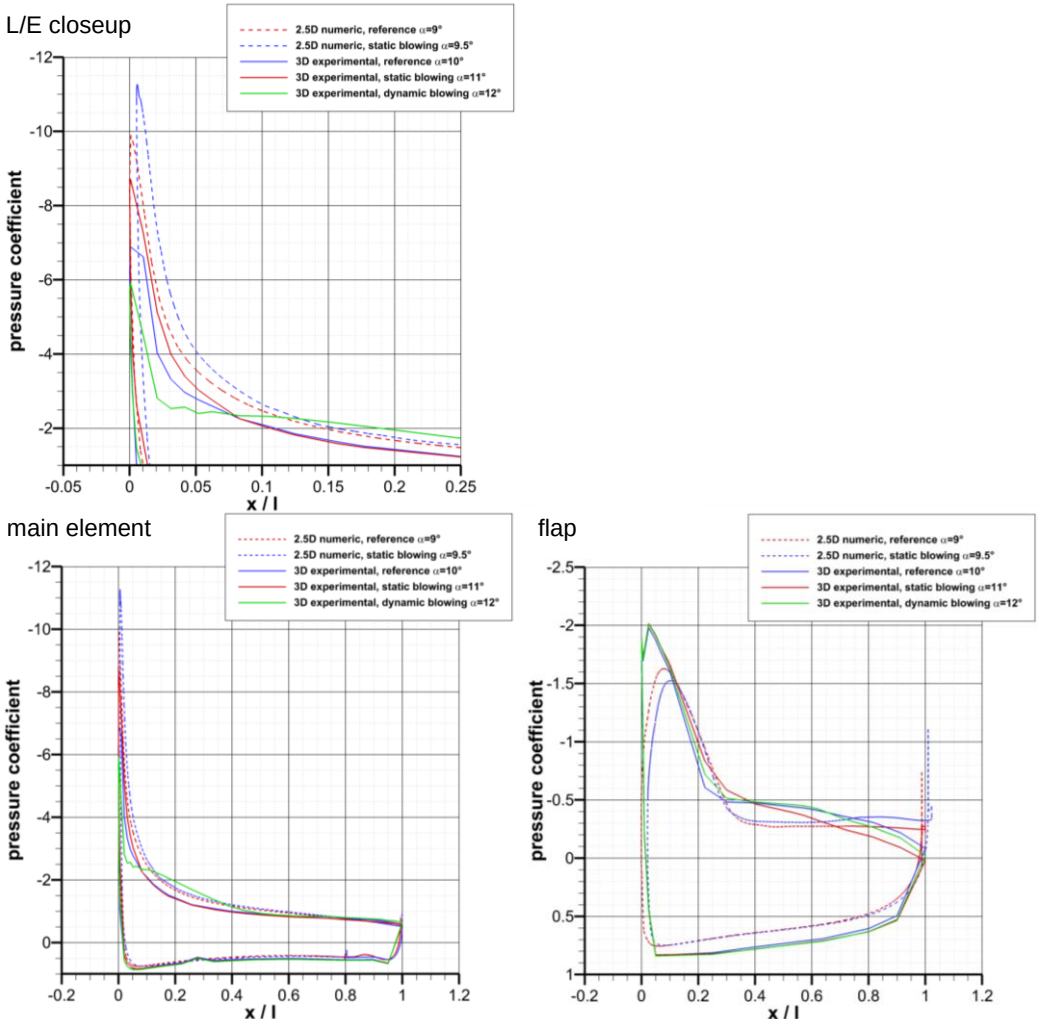

Fig. 1: Pressure distributions of AFC cases at the respective AoA of maximum lift coefficient; airfoil center section

the other (experimental as well as numerical) cases it shows a very reduced suction peak and some kind of “hump” in the mid-region (x/l = 0.1…0.4) of the main element. Based on the observation of similar effects in other experimental results one can conclude that this is due to a turbulent leading edge separation, which is forced by the dynamic blowing using an effect called “post stall flow control” [1], which is an advantegeous effect, but however not the kind of effect that is desired in this framework.

A comparison of the numerical result without and with AFC and the experimental result (static blowing) without and with AFC reveals very similar phenomenology: In both cases the suction peak is increased significantly, while there is only minor change of the C_P-distribution along the remaining airfoil surface. Also quantitatively the increase of minimum pressure in the suction peak ($\Delta C_{P,min} \approx 1.5$) is similar. Hence in the center section of the airfoil—which is some distance away from the wingtip as well as from the windtunnel wall—the 2.5D active flow control computations are well able to predict similar phenomenology and similar trends. This in turn also means that the 3D experimental setup does successfully represent an infinite swept airfoil in it’s center section.

6 References

[1] P. Scholz, M. Casper, J. Ortmanns, C.J. Kähler and R. Radespiel: Leading-Edge Separation Control by Means of Pulsed Vortex Generator Jets, AIAA Journal, 46(4), p. 837, 2008

[2] P. Scholz, C.J. Kähler, R. Radespiel, J. Wild, and G. Wichmann: Active Control of Leading-Edge Separation within the German Flow Control Network, 47th AIAA Aerospace Sciences Meeting, Orlando, USA, 2009

[3] J. Wild, G. Wichmann, F. Haucke, I. Peltzer, and P. Scholz: Large Scale separation flow control experiments within the German Flow Control Network, 47th AIAA Aerospace Sciences Meeting, Orlando, USA, 2009

[4] P. Scholz, S. Mahmood, M. Casper, R. Radespiel, M. Sitzmann, and V. Ciobaca: Experimental and Numerical Investigations on the Control of Airfoil Stall using Vortex Generator Jets, 5th Flow Control Conference, Chicago, Illinois, 2010

[5] M. Casper, P. Scholz, R. Radespiel, J. Wild and V. Ciobaca: Separation control on a High-Lift Airfoil using Vortex Generator Jets at High Reynolds numbers, 41st AIAA Fluid Dynamics Conference and Exhibit, Honolulu, Hawaii, 2011.

[6] J. Wild: Experimental investigation of Mach- and Reynolds-number dependencies of the stall behaviour of 2-element and 3-element high-lift wing sections, 50th AIAA Aerospace Science Meeting, Nashvill, Tennessee, 2012

[7] G. Godard and M. Stanislas: Control of a decelerating boundary layer. Part 1: Optimization of passive vortex generators, Aerospace Science and Technology, 10(6), p.181, 2006

[8] S.S. Mahmood, P. Scholz and R. Radespiel: Numerical Design of Leading Edge Flow Control over Swept High-Lift Airfoil, 3rd CEAS Air&Space Conference / 21st AIDAA Congress, Venice, Italy, 2011

[9] T. Naveh, A. Seifert, A. Tumin and I. Wygnanski: Sweep Effect on Parameters Governing Control of Separation by Periodic Excitation, Journal of Aircraft, 35(3), p.510

[10] J.Z. Wu, X.Y. Lu, A.G. Denny, M. Fan, J.M. Wu: Post-stall Flow Control on an Airfoil by Local Unsteady Forcing, Journal of Fluid Mechanics, 371, p.21

[11] D. Schwamborn, T. Gerhold, R. Heinrich: The DLR TAU-Code: Recent Applications in Research and Industry, *In: P. Wesseling, E. Oate, J. Priaux (Eds), ECCOMAS CFD*, *Egmond aan Zee*, The Netherlands, 2006.

[12] Commercial CFD software by POINTWISE, Inc. http://www.pointwise.com/gridgen

[13] S.S. Mahmood, R. Radespiel: RANS simulation of jet actuation in a boundary layer flow using Chimera grids, *Deutscher Luft- und Raumfahrtkongress*, Aachen, Germany, 8-10 Sep, 2009.

[14] P.R. Spalart, S.R. Allmaras: A one-equation turbulence model for aerodynamic flows, *La Rech.*, Aerospatiale No.1, 1994, pp. 5-21.

[15] F.R. Menter: Zonal two-equation k-w turbulence model for aerodynamic flows, *AIAA paper*, AIAA 93-2906, 1993.